

Three particle correlation functions for an electrolyte: theory and molecular simulation results

Felipe Jimenez-Angelos,^{1,2}, Rene Messina,^{3,y} Christian Holm,^{3,z} and Marcelo Lozada-Cassou^{1,2,x}

¹Programa de Ingeniería Molecular, Instituto Mexicano del Petróleo,
Lázaro Cárdenas 152, 07730 México, D. F., México

²Departamento de Física, Universidad Autónoma Metropolitana-Iztapalapa, Apartado Postal 55-334, 09340 D. F. México

³Max-Planck-Institut für Polymerforschung, Ackermannweg 10, 55128 Mainz, Germany

(Dated: February 7, 2020)

The three point extension to the hypernetted chain/mean spherical approximation (TPE-HNC/MSA) integralequations is applied to the restricted primitive model electrolyte. The obtained three particle correlation functions $g^{(3)}(r_1; r_2; r_3)$, for the long range and the short range correlated (symmetric) electrolyte, show good agreement with molecular dynamics (MD) simulation. The effective mean force between two ions (which is related to the pair correlation function) is computed from the projection of $g^{(3)}(r_1; r_2; r_3)$ through an exact theorem of force balance. The forces obtained by TPE-HNC/MSA, HNC/MSA and MD are compared and, as a major result, the best agreement is found between TPE-HNC/MSA and MD due to the better incorporation of long range correlations by TPE.

PACS numbers: 61.20.Gy, 61.20.Qg, 61.20.Ja

I. INTRODUCTION

In a N -particle uid, the n -particle distribution function, $g^{(n)}(r_1; \dots; r_n)$, gives the probability density to find n particles in a given con guration $r_1; \dots; r_n$ independently of the remaining $N - n$ particles. Its computation is the objective of the classical statistical mechanics of uids, and it is of fundamental importance to understand, at the molecular level, thermodynamical properties of uids [1, 2, 3]. The homogeneous uid two-particle distribution function, $g^{(2)}(r_1; r_2)$, is related with the structure factor, $S(k)$, through the inverse Fourier transform. The $S(k)$ function can be measured, for example, by neutron scattering experiments in molecular uids [4]. In colloidal systems, $g^{(2)}(r_1; r_2)$ can be measured directly by optical microscopy. Measurements of $g^{(2)}(r_1; r_2)$ have been used recently to compute the effective force between confined colloidal particles [5, 6].

In theoretical calculations, several approaches have been proposed for the study of homogeneous uids: hierarchy equations [7, 8, 9], density functionals [10, 11], the integral equations formalism [12, 13] and molecular simulation methods such as Monte Carlo (MC) [14] and Molecular Dynamics (MD) [15] which are considered as exact and therefore used as a reference for theories. In all these approaches, $g^{(2)}(r_1; r_2)$, is the key observable. In hierarchy equations, such as Born-Green-Yvon (BGY) and Kirkwood equations, $g^{(n)}$ is expressed in terms of $g^{(n+1)}$ and therefore a closure between the two functions is needed. A classical closure used in hierarchy equations

is the Kirkwood superposition approximation (KSA) [9]. In KSA, pair wise additivity is assumed on the level of the potential of mean force. For some systems under certain conditions KSA provides a suitable description. However this is not always true. For example, for a dense hard spheres uid [1, 16] and for highly correlated model electrolytes [17], the comparison of BGY with molecular simulation data is not satisfactory.

The density functional approaches are based on the idea that the free energy of an inhomogeneous uid can be expressed as a functional of density. Thereby, all the relevant thermodynamical properties of a system can be computed. This formalism was mainly developed for inhomogeneous uids in the early 60's [10, 11, 18, 19, 20]. It has been also successfully applied to homogeneous uids. In the integral equations formalism, the total correlation function $h(r)$ and the direct correlation function $c(r)$ are linked via the Ornstein-Zernike (OZ) integralequation. To solve the OZ equation a closure relationship between $c(r)$ and $h(r)$ must be given. Depending on the closure, different integral equation theories can be derived. Some of the well known are the Percus-Yevick (PY) [21], hypernetted chain (HNC) [22] and mean spherical (MSA) [23] approximations. More recently, hybrid theories such as the hypernetted chain /mean spherical approximation (HNC/MSA) have been applied to bulk uids [24]. These integralequation theories can also be derived through the density functionals formalism by choosing a suitable free energy function [25]. All of these approaches ignore different types of diagrams in the Mayer expansion [26, 27], i. e., some correlations are ignored. Integral equations theories are formal in the sense that it is known what class of diagrams are ignored. Hence, comparisons with molecular simulations are needed to quantify the accuracy of the approximations. For example, a comparison of HNC and PY calculations with molecular simula-

^xElectronic address: fangelos@www.imp.mx

^yElectronic address: messina@mpip-mainz.mpg.de

^zElectronic address: holm@mpip-mainz.mpg.de

^xElectronic address: marcelo@www.imp.mx

tion results for the thermodynamical properties of a hard sphere uid shows an improvement with respect to hierarchy theories but still fail at high uid concentrations [1, 16].

Concerning integralequations theories, it has been proposed a method to systematically incorporate higher order molecular correlations [27, 28]. This approach makes use of the equivalence between particles and uids where an external uid is considered as one more uid species at infinite dilution [29]. This simple idea can be applied to the concept of an external uid artificially produced by two fixed particles. Then, the obtained uid distribution function is a conditional three-particle distribution function denoted as $g^{(3)}(r_1; r_2; r_3)$, i.e., the probability density to find a third particle (located at r_3 , see Fig. 2) when there are two fixed particles (located at r_1 and r_2) [30, 31, 32]. By projecting this triplet correlation function one gets the mean effective force between two interacting particles and the pair distribution function $g^{(2)}(r_1; r_2)$. The resulting pair distribution function is obtained with more included correlations and it might provide a better system description. This method is a three point extension (TPE) to integralequation theories.

TPE to integral equation theories has been successfully applied to compute the effective force between two charged parallel plates immersed in a restricted primitive model (RPM) electrolyte [30, 31, 32]. It is found that TPE better describes the computed force between two charged parallel plates than the conventional HNC/M SA and KSA [32]. Comparisons of TPE with MC and MD for the effective force between two plates immersed into a hard spheres [33] uid and a RPM electrolyte [34, 35] show an excellent agreement. TPE to the integral version of the Poisson-Boltzmann equation has been applied to compute the effective force between two like charged spherical colloids immersed into a point ions electrolyte [36, 37, 38, 39]. A shortcoming of these studies, however, is that the interacting macroparticles are considered at infinite dilution.

For the homogeneous RPM electrolyte, studies on its thermodynamical properties have been done using the HNC [40, 41, 42], M SA [43, 44], HNC/M SA [24] and BGY [17] theories, as well as MC simulations [45, 46]. From these studies it is found that all these theories describe well the RPM in certain regimes. Nonetheless, they all fail in the regime of dilute multivalent ions where long range correlations are important [24, 42, 47]. Especially it is well known the appearance of a spurious peak in the HNC coion radial distribution function for dilute divalent electrolytes [24, 47]. To try to solve this problem different approximations to the, so-called, bridge function, B , have been proposed in the past by Rossky et al. [48] and Haym et al. [49, 50, 51, 52]. However, these bridge functions unfortunately overcorrect the peak, and the results are not satisfactory when compared to computer simulations.

An approach, to study inhomogeneous integral equa-

tions for a uid next to a plate have been developed by Kjellander et al. [53] and Pischke and Henderson [54, 55] where they calculated the two-particle, inhomogeneous distribution function. More relevant for this work, however, is that of Attard [56, 57], who calculated the two-particle inhomogeneous distribution function, through the Percus-Yevick (PY) approximation for a hard sphere uid next to a spherical external uid (produced by a hard sphere particle). In his approach, if the spherical external uid is of the same size as the rest of the particles, one obtains the triplet correlation function for hard spheres. He finds an excellent agreement with MC data. However, to the best of our knowledge, no triplet correlation function has been calculated for the RPM. On this basis, one can state that a theory for a simple charged uid, that properly includes these long ranged correlations is needed.

The aim of this paper is to show that by including more correlations through the TPE method, it is obtained a better description of a simple charged uid, i.e., the RPM electrolyte. The structure of the article is set out as follows. In Sec. II we present the TPE formalism. Section III is devoted to the computational details of the MD simulation. In Sec. IV, we present our results for two typical (divalent) electrolyte concentrations. The obtained $g^{(3)}(r_1; r_2; r_3)$ with TPE and MD simulation are compared. We also compare the mean force between two particles obtained with TPE, conventional HNC/M SA and MD. Finally, Sec. V contains concluding remarks.

II. THEORY

A. Three point extension to integral equation theories

The pair correlation function, $g(r_{12} | r_1, r_2)$, of a one-component uid with its components interacting through the pair potential $u(r_{12})$, is related to the potential of mean force $w(r_{12})$ (between two particles located at r_1 and r_2) by

$$g(r_{12}) = \exp f \quad w(r_{12})g : \quad (1)$$

If $g(r_{12})$ is expanded in powers of the bulk concentration, the n -th order coefficient is a sum of integrals of products of the Mayer function $f(r_{12}) = \exp f - u(r_{12}) - 1$. Such an integral of a product of M Mayer functions can be conveniently represented by Mayer diagrams [1, 26, 27]. The diagrams of the first and second order coefficients are given in the left hand side of Fig. 1. There is still not an exact theory to compute $g(r_{12})$, and all the available theories ignore several classes of topologically different diagrams. We will come back to this point below when we discuss the direct correlation function and the Ornstein-Zernike equation. In a multi-component uid, the total correlation function, $h_{ij}(r_{12}) = g_{ij}(r_{12}) - 1$, between

two particles of species i and j located at r_1 and r_2 , respectively, is related to the direct correlation function, $c_{ij}(r_{12})$, through the Ornstein-Zernike equation which for a k -component uid is given by

$$h_{ij}(r_{12}) = c_{ij}(r_{12}) + \sum_{m=1}^{X^k} h_{im}(r_{23}) c_{mj}(r_{13}) dr_3; \quad (2)$$

where c_m is the concentration of species m . Several closures between $h_{ij}(r_{12})$ and $c_{ij}(r_{12})$ have been proposed, for instance,

$$c_{ij}(r_{12}) = u_{ij}(r_{12}) + h_{ij}(r_{12}) \ln g_{ij}(r_{12}); \quad (3)$$

$$c_{ij}(r_{12}) = u_{ij}(r_{12}); \quad \text{and} \quad (4)$$

$$c_{ij}(r_{12}) = f_{ij}(r_{12}) g_{ij}(r_{12}) \exp f_{ij}(r_{12}) g: \quad (5)$$

Equations (3), (4) and (5) are known as the hypermetted chain equation (HNC), the mean spherical approximation (MSA) and the Percus-Yevick (PY) equation, respectively. In the hypermetted chain theory, the bridge diagrams are ignored whereas in the Percus-Yevick approximation both the bridge and product diagrams are neglected [1, 2]. The first and second order Mayer graphs of the HNC and PY theories are also given in Fig. 1.

Let us now propose [27, 30] that in a uid of k -species there is an additional dumbbell species at infinite dilution made up of two particles (of species i and j) at fixed relative position $\tau = r_{12}$ (see Fig. 2). By defining the dumbbell species as τ , we now have a $(k+1)$ -component uid. For $\tau \neq 0$, the total correlation function between the particle of species i and the uid particle of species j reads

n	Exact	HNC	PY
1			
2			

FIG. 1: Mayer diagrams for the first ($n = 1$) and second ($n = 2$) order in expansion of the pair correlation function, $g^{(2)}(r)$. The exact, hypermetted chain (HNC) and Percus-Yevick (PY) coe cients are shown. The black points and white dots are called eld and root points, respectively. The bonds represent the Mayer function $f(r_{12})$.

$$h_{ij}(r_3) = c_{ij}(r_3) + \sum_{m=1}^{X^k} h_{im}(r_{34}) c_{mj}(r_{34}) dr_4; \quad (6)$$

where $c_{mj}(r_{34})$ is the direct correlation function between particles of species m and j both different from i . In order to obtain $c_{mj}(r_{34})$, the k -component Ornstein-Zernike equation [Eq. (2)] has to be used. Different integral equation theories [27] can be obtained depending on the closure relations used for $c_{ij}(r_3)$ and $c_{mj}(r_{34})$ in Eq. (6). For instance, TPE-HNC/MSA is obtained if MSA [Eq. (4)] is used for $c_{mj}(r_{34})$ and HNC [Eq. (3)] for $c_{ij}(r_3)$.

In this formalism, the distribution function, $g_i(r_3)$, of the i species around the τ species can be interpreted as a conditional three-particle distribution function denoted by $g_{-i}^{(3)}(r_1; r_2; r_3; t = r_1 - r_2)$, i.e., the density probability of finding a particle of species i at r_3 in the presence of the dumbbell. Mathematically the conditional three-particle distribution function, $g_{-i}^{(3)}(r_3; t)$, is related to the homogeneous three-particle distribution function $g_{-i}^{(3)}(r_1; r_2; r_3)$ by

$$g_{-i}^{(3)}(r_3; t) = \frac{g_{-i}^{(3)}(r_1; r_2; r_3)}{g^{(2)}(t)}: \quad (7)$$

The projection of $g_{-i}^{(3)}(r_1; r_2; r_3)$ gives directly $g^{(2)}(t)$. This projection can be provided by the Boltzmann-Green-Yvon theorem (BGY) that is based on a balance of the mean effective force $F = \nabla g_{-i}^{(3)}(r_3; t)$.

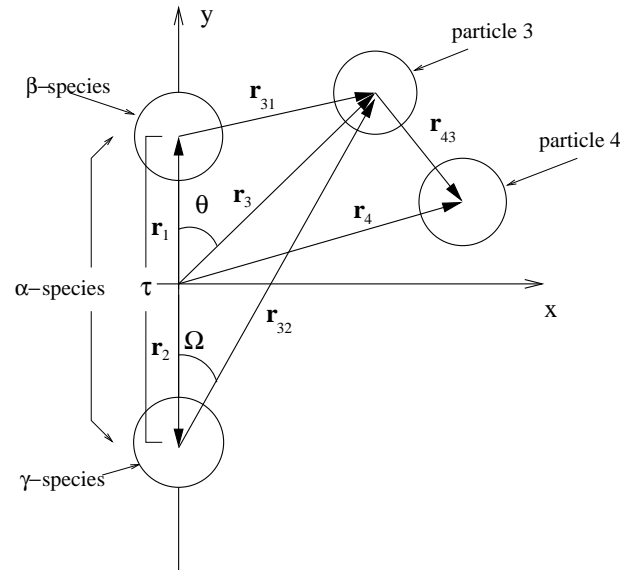


FIG. 2: Schematic representation of the model.

B. The Born-Green-Yvon equation or a force law

The Born-Green-Yvon (BGY) equation is one of the so called hierarchy equations and it is an exact theorem relating the n and $(n+1)$ particle distribution functions [7, 8]. Here, we derive the BGY equation as a sum of all the forces exerted on one of the two dumbbell's particles (let us say particle of species i at r_2). This mean force has two contributions: (i) the direct force $f_i(t)$ exerted by the particle of species i at r_2 and (ii) the force $f^d(t)$ exerted by all the other particles. Thereby, the total mean force $F(t)$ reads

$$F(t) = f_i(t) + f^d(t); \quad (8)$$

Assuming that the dumbbell and uid species are spherical particles interacting through central force potentials, the component of f along t is given by

$$f_i(t) = \frac{du_i(t)}{d}; \quad (9)$$

where $u_i(t)$ is the potential of direct interaction between the two dumbbell particles. The elementary force df^d produced by a uid element at r_3 is given by $df^d = \sum_{i=1}^{X^k} f_i(r_{23}) u_i(r_3) dv_3$, where $f_i(r_{23})$ is the force between a particle of species i of local density $u_i(r_3)$ $ig^{[3]}_i(r_3; \cdot)$ at r_3 and the dumbbell's test particle of species i . The component of df^d along the direction of t is given by

$$df^d = \sum_{i=1}^{X^k} \hat{t} \cdot f_i(r_{23}) u_i(r_3) dv_3 \\ = \sum_{i=1}^{X^k} \hat{t} \cdot \hat{r}_{23} \frac{du_i(r_{23})}{dr_{23}} u_i(r_3) dv_3; \quad (10)$$

with \hat{t} and \hat{r}_{23} being unit vectors along the t and r_{23} directions, respectively, $u_i(r_{23})$ is the potential of interaction between an i -species particle with the $-$ -species particle. Substituting Eqs. (9) and (10) into Eq.(8), F is given by

$$F(t) = \frac{dw(t)}{d} = \frac{du_i(t)}{d} \\ + \sum_{i=1}^{X^k} \frac{du_i(r_{23})}{dr_{23}} \cos g^{[3]}_i(r_3; \cdot) dv_3; \quad (11)$$

where $\hat{t} \cdot \hat{r}_{23} = \cos \theta$ and $w(t)$ is the potential of mean force between the two dumbbell's particles. According to Eq. (1),

$$w(t) = k_B T \ln g(t); \quad (12)$$

and thus

$$k_B T \frac{d \ln g(t)}{d} = \frac{du_i(t)}{d} \\ + \sum_{i=1}^{X^k} \frac{du_i(r_{23})}{dr_{23}} \cos g^{[3]}_i(r_3; \cdot) dv_3; \quad (13)$$

which is the Born-Green-Yvon (BGY) equation. The degree of accuracy of $g(t)$ depends on the method used to compute $g^{[3]}_i(r_3; \cdot)$. If $g^{[3]}_i(r_3; \cdot)$ is computed through the TPE of integral equation theories, it was shown that new diagrams are included in the cluster expansion of $g^{(2)}(\cdot)$ [27] (see Fig. 3). By examination of the transformation of the Mayer diagrams through the formalism outlined above, the denomination of three point extension becomes clear.

C. Application to the RPM electrolyte

In the RPM electrolyte the uid is considered as made up of hard spheres of diameter a with a central charge $q_i = z_i e$, where z_i is the valence of species i and e is the protonic charge. The electroneutrality condition for the n-component electrolyte is

$$\sum_{i=1}^{X^n} z_i = 0; \quad (14)$$

Assuming that the dumbbell particle (i species) is made up of two particles of the same species from that in the uid (see Fig. 2), the TPE-HNC/MSA equations become

$$g_{i,i}(r_3) = \exp \left(\sum_{X^k} \frac{u_{i,i}(r_3)}{Z} \right) \\ + \sum_{m=1}^{X^k} h_m(r_4) c_{m,i}(r_{34}) dr_4; \quad (15)$$

where

$$u_{i,i}(r_3) = \frac{u_{i,i}(r_{13}; r_{23})}{8} \\ \gtrapprox \frac{z_i z_j e^2}{r_{23}} + \frac{z_i z_j e^2}{r_{13}} \text{ if } r_{13} \text{ and } r_{23} > a \\ \gtrapprox 1 \text{ if } r_{13} \text{ or } r_{23} < a \quad (16)$$

with z_i and z_j standing for valence number of particles i and j , respectively. For spherical ions the direct correlation function depends only of the ions distance $r_{34} = |r_{34}|$: Within the mean spherical approximation, its analytic expression is

$$c_{m,i}(r_{34}) = c^{hs}(r_{34}) + z_m z_i c^{sr}(r_{34}) \frac{z_m z_i e^2}{r_{34}}; \quad (17)$$

where $c^{hs}(r_{34})$ is the direct correlation function for a hard spheres uid in the PY approximation and $c^{sr}(r_{34})$ is a

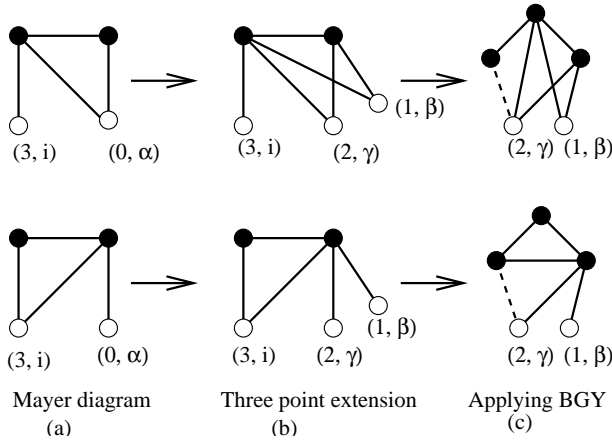


FIG. 3: Two examples of the transformation of Mayer diagrams under TPE. The notation for the particles and species is the same as in Fig. 2. The dashed bond represents the $f_{i,j}(r_{23}) = \frac{du_{i,j}(r_{23})}{dr_{23}}$ function. Thereby, in (N, \cdot) , N stands for the particle number and \cdot for the particle species (see also Fig. 2). $N = 0$ stands for the dumbbell particle. (a) An example of a second order Mayer diagram involving a dumbbell particle and particle 3. (b) The same diagram as in (a) but the constitutive particles of the dumbbell are explicated, i.e., at the level of the triplet correlation function. (c) Resulting diagrams upon applying BGY (on the level of the mean force).

short ranged function. Because of the symmetry around the dumbbell axis, it is convenient to use prolate coordinates (x, y, z) [57, 58] defined as follows

$$\begin{aligned} x &= \frac{p}{2p} \frac{(\frac{p}{2} - 1)(1 - \frac{p}{2})}{(\frac{p}{2} + 1)(1 + \frac{p}{2})} \cos \theta; \\ y &= \frac{p}{2} \frac{(\frac{p}{2} - 1)(1 - \frac{p}{2})}{(\frac{p}{2} + 1)(1 + \frac{p}{2})} \sin \theta; \\ z &= \frac{1}{2}; \end{aligned} \quad (18)$$

and where the volume element is given by

$$dv = \frac{3}{8} r^2 \sin^2 \theta d\theta d\phi d\psi. \quad (19)$$

The relative distance r_{34} is then given by

$$\begin{aligned} r_{34}^2 &= \frac{2}{4} \left(\frac{2}{3} - 1 \right) \left(1 - \frac{2}{3} \right) + \frac{2}{4} \left(1 - \frac{1}{3} \right) \left(1 - \frac{2}{4} \right) \\ &+ \frac{1}{2} \frac{\left(\frac{2}{3} - 1 \right) \left(1 - \frac{2}{3} \right) \left(\frac{2}{4} - 1 \right) \left(1 - \frac{2}{4} \right)}{\left(\frac{2}{3} - 1 \right) \left(1 - \frac{2}{3} \right) \left(\frac{2}{4} - 1 \right) \left(1 - \frac{2}{4} \right)} \cos \theta; \end{aligned} \quad (20)$$

In prolate coordinates the potential of electrostatic interaction, $u_{i,j}^{el}$, between the dumbbell and one uid ion of species i can be conveniently rewritten as

$$u_{i,j}^{el}(\theta, \phi) = \frac{2e^2}{\pi} \frac{z}{r_{34}^2} + \frac{z}{r_{34}^2}; \quad (21)$$

and Eq. (16) as

$$\begin{aligned} g_{i,j}(3; 3) &= g_{i,j}^{[3]}(3; 3; 3) \\ &= \exp \frac{2e^2}{\pi} \frac{z}{r_{34}^2} + \frac{z}{r_{34}^2} \\ &+ \frac{1}{Z_1 Z_1} s(4; 4) \\ &+ \frac{K(3; 3; 4; 3) d_4 d_4}{Z_1 Z_1} \\ &+ z_1 \frac{1}{Z_1 Z_1} d(4; 4) \\ &+ \frac{L(3; 3; 4; 4) d_4 d_4}{Z_1 Z_1} \\ &+ \frac{A(3; 3; 4; 4) d_4 d_4}{Z_1 Z_1} \\ &+ J(3; 3) g; \end{aligned} \quad (22)$$

with

$$o(\theta) = \begin{cases} +b & \text{for } 0 < \theta < 1 \\ 1 & \text{for } 0 < \theta < 0 \end{cases}$$

and $b = 1$, $b = 2a$ and $o(\theta) = o(\theta)$. The expressions for K, L, A, J, s and d are

$$\begin{aligned} K(3; 3; 4; 4) &= \frac{3}{8} \left(\frac{2}{4} \frac{2}{4} \right) \max_{Z_0} C^{hs}(r_{34}) d_4; \\ L(3; 3; 4; 4) &= \frac{3}{8} \left(\frac{2}{4} \frac{2}{4} \right) \max_{Z_0} C^{sr}(r_{34}) d_4; \\ A(3; 3; 4; 4) &= \frac{4e^2}{8\pi} \left(\frac{2}{4} \frac{2}{4} \right) \frac{Z_2}{0} \frac{d_4}{r_{34}}; \\ s(4; 4) &= \frac{X^n}{m=1} \frac{z_m h_m}{m} (4; 4); \\ d(4; 4) &= \frac{X^n}{m=1} \frac{z_m h_m}{m} (4; 4); \end{aligned}$$

$$\begin{aligned} J(3; 3) &= \frac{Z_{m \in (1)} Z_{0(4)}}{Z_1 Z_{0(4)}} K(4; 4; 3; 3) d_4 d_4 \\ &+ \frac{1}{Z_{m \in (1)}} K(4; 4; 3; 3) d_4 d_4; \end{aligned}$$

respectively, with

$$m \in (1) = \begin{cases} 0 & \text{if } a \\ 0 & \text{if } a > a \end{cases}$$

By introducing the elliptic function of second kind $F(-2; k)$, one can rewrite A as

$$A(3; 3; 4; 4) = \frac{\frac{2}{3} \frac{2}{3} F(-2; k)}{2r_{34}^{m \in (1)}} \quad (23)$$

where

$$k^2 = \frac{2^2 p}{2(r_{34}^{\text{max}})^2} \frac{\left(\frac{2}{3} - 1\right)\left(1 - \frac{2}{3}\right)\left(\frac{2}{4} - 1\right)\left(1 - \frac{2}{4}\right)}{\left(\frac{2}{3} + 1\right)\left(1 + \frac{2}{3}\right)}, \quad (24)$$

and

$$\begin{aligned} (r_{34}^{\text{max}})^2 &= \frac{2}{4} \frac{q}{\left(\frac{2}{3} - 1\right)\left(1 - \frac{2}{3}\right)} \\ &+ \frac{q}{\left(\frac{2}{4} - 1\right)\left(1 - \frac{2}{4}\right)}^2 \\ &+ \left(\frac{3}{3} - \frac{4}{4}\right)^2 : \end{aligned} \quad (25)$$

Using Eq. (11), the mean force between the two dumbbells particles reads

$$F(r) = f(r) + f^{\text{el}}(r), \quad (26)$$

where

$$\begin{aligned} f(r) &= \frac{2}{2} \sum_{j=1}^2 \frac{Z_1}{Z_j} g_{\text{in}}^{[3]}(r) \\ &+ \frac{2}{3} \frac{3b_3^2 + 2b^2}{3b_3^2 + b^2} d_3 : \end{aligned} \quad (27)$$

and

$$\begin{aligned} f^{\text{el}}(r) &= \frac{z z_3 e^2}{\pi^2} + \frac{z e^2}{\pi} \frac{Z_1 Z_3}{1 - \cos(r)} d_3 \\ &+ \frac{(1 - z_3 z_3)(z_3 + z_3)}{(z_3 - z_3)^2} d_3 d_3 : \end{aligned} \quad (28)$$

Thus the pair distribution function of the electrolyte solution is given by

$$g(r) = \exp \left[- \int_1^r F(r') dr' \right] : \quad (29)$$

The solution of Eq. (22) and calculation of F through Eqs. (26), (27) and (28) have to be numerically computed (see the appendix for the finite element method).

III. MOLECULAR DYNAMICS

The electrolyte is confined in a cubic box of length L . The bulk salt concentration is then given by $\frac{N}{L^3}$, where N is the number of positive (or negative) ions. The dumbbell is made up of two fixed ions (with a center-center separation r) disposed symmetrically along the axis passing by the two centers of opposite faces. A similar system setup was also used elsewhere to study two fixed macroions [59, 60, 61]. We use MD simulations to compute the motion of the mobile fluid ions coupled to a heat bath acting through a weak stochastic force $W_i(t)$

with a zero mean value. The equation of motion of any mobile ion i reads

$$m \frac{d^2 r_i}{dt^2} = r_i U - m \frac{dr_i}{dt} + W_i(t); \quad (30)$$

where m is the ion mass, U is the friction coefficient and $r_i U$ is the potential force having two contributions: (i) the Coulomb interaction and (ii) the excluded volume interaction. Friction and stochastic force are linked by the dissipation- fluctuation theorem $W_i(t) = W_j(t^0) e^{i(t-t^0)} = 6m k_B T_{ij} e^{i(t-t^0)}$.

Excluded volume interactions are modeled by a pure repulsive Leonard-Jones (LJ) potential defined by

$$U_{\text{LJ}}(r) = \begin{cases} \frac{8}{4} \frac{a}{r}^{12} - \frac{a}{r}^6 & \text{for } r < 2^{1/6}a \\ 0; & \text{for } r > 2^{1/6}a; \end{cases} \quad (31)$$

where a is the ion diameter.

The electrostatic interaction between any pair ij , where i and j denote either a dumbbell ion and/or a mobile fluid ion, reads

$$U_{\text{el}}(r) = k_B T_B \frac{z^2}{r}; \quad (32)$$

where $+ (-)$ applies to ions likely (oppositely) charged, $\lambda_B = \frac{e^2}{8\pi k_B T}$ is the Bjerrum length describing the electrostatic strength and z is the salt valence ($z_i = z_j = z$). To link our system parameters to experimental units we choose the LJ energy parameter $\lambda_{\text{LJ}} = k_B T$ (where $T = 298\text{K}$) and $a = 4.25\text{\AA}$. This leads then to the water Bjerrum length $\lambda_B = 1.68a = 7.14\text{\AA}$. A macroscopic system was modeled by imposing periodic boundary conditions. The long range Coulomb interaction was treated by using an optimized and efficient Ewald summation variant, namely the particle-particle-particle-mesh (PPM) method [62].

In order to limit the size effects, we choose L sufficiently large, typically 10 times (or more) the Debye-Hückel screening length. The number of ions in the box is 500 for all cases (concentrated and dilute solutions). It is important to mention that the computation of $g_{ij}^{[3]}(r; \theta)$ is statistically extremely demanding and especially for small angles, since the quantity of information varies like $\sin(\theta)$. In this notation, the distance $r = r_3$ and the angle $\theta(r_1, r_3)$ are always relative to the center of the dumbbell (see Fig. 2). The fact that the observable $g_{ij}^{[3]}(r; \theta)$ concerns only an "elementary solid angle", it strongly reduces the available information compared to that available for the pair correlation function, since in that latter case a full solid angle 4π and many ion pairs are accessible. To overcome to this difficulty, we considered a sufficiently large angle range

(typically between 5–15⁰ depending on the concentration), so that the gathered informations contains as less noise as possible. On the other hand, m must not to be too large otherwise the resolution gets too small. For each system under consideration, a compromise between these two effects that had to be found.

Finally for the computation of the effective mean force between two ions, we considered the same system but where no fixed dumbbell is present. Thereby, we could compute the potential of mean force, knowing the $g(r)$, and then get by derivation the effective force.

IV. RESULTS

We have done calculations for the 1:1 and 2:2 electrolytes. For the 1:1 electrolyte the agreement between TPE and MD results is quantitatively very good. However, in order to keep low the number of plots we just present a detailed analysis on the results of the 2:2 electrolyte. The choice of divalent ions is motivated by the fact that it represent a strong test for the TPE–HNC/M SA theory. Thereby, we considered two typical concentrations: (i) the concentrated case with $\rho = 1\text{M}$ and (ii) the dilute case with $\rho = 0.005\text{M}$. As a main result, the effective mean force obtained by TPE–HNC/M SA, HNC/M SA, and MD simulation is presented for each concentration regime. In order to further quantify the robustness of the TPE theory, we investigated in detail the conditional three-particle distribution function, $g_{+i}^{[3]}(r; \theta)$, by comparing TPE with MD.

For the discussion, it is convenient to adopt the following notations: $g_{++}^{[3]}(r; \theta)$ stands for the distribution function of negative ions when the dumbbell is made up of two positive ions, $g_{+-}^{[3]}(r; \theta)$ for that of negative ions when the dumbbell is made up of a negative and a positive ions, and so on. By symmetry the three-particle distribution function satisfies $g_{++}^{[3]}(r; \theta) = g_{+-}^{[3]}(r; \theta)$ and also $g_{+-}^{[3]}(r; \theta) = g_{-+}^{[3]}(r; \theta)$. Thereby, we systematically compared theory and simulation for $g_{+i}^{[3]}(r; \theta = a)$ (i.e., when the two dumbbell ions are in contact) for two given values of θ ($= 4$ and $= 2$). Besides, within TPE theory, we also provide the full θ -dependence of $g_{+i}^{[3]}(r; \theta)$ for different θ .

A. Concentrated case

In this section, we deal with the concentrated electrolyte solution ($\rho = 1\text{M}$). The electrostatic screening at such high ionic density and valence ($z = 2$) is very strong. The study of such a system is important to test TPE–HNC/M SA theory, since already inhomogeneous and homogeneous HNC/M SA theories are in excellent agreement with molecular simulations under such conditions [63].

1. Three particle correlation function

a. Symmetric dumbbell We first consider symmetric dumbbells made of like charged positive divalent ions. The profiles of $g_{++}^{[3]}(r; \theta = 2; \theta = a)$ and $g_{++}^{[3]}(r; \theta = 4; \theta = a)$ are depicted in Fig. 4. Concerning the negatively charged uid ions (i.e., “dumbbell counterions”), we have quantitative agreement between theory and simulation even near the distance of closest approach. The slight difference at short distance ($r < a$) is due to the fact that for the short-ranged excluded volume interaction, MD simulation is built with a soft-core LJ potential whereas the actual theory uses a true hard-core potential. For the positively charged uid species (“dumbbell counterions”), we also have an excellent qualitative agreement. The TPE maximum of the cion distribution function is within the statistical error however slightly higher than MD data. The location of the maximum is nearly the same as that found with simulation. Hence, although TPE has an excellent agreement with MD, probably TPE slightly overestimates the local cion concentration near the dumbbell.

For $\theta = 4$ (see Fig. 5), one still has the same quantitative agreement between MD and TPE for the dumbbell-counterions. It is observed that the value of $g_{++}^{[3]}(r; \theta = 4; a)$ at closest approach ($r = 1.29a$) is not as high as at $\theta = 2$ (see Fig. 4) for the corresponding plot. The physical reason of this feature is straightforward. The closest approach to the center of the dumbbell is larger at $\theta = 4$ than at $\theta = 2$, therefore, since all particles have the same size, the resulting attractive

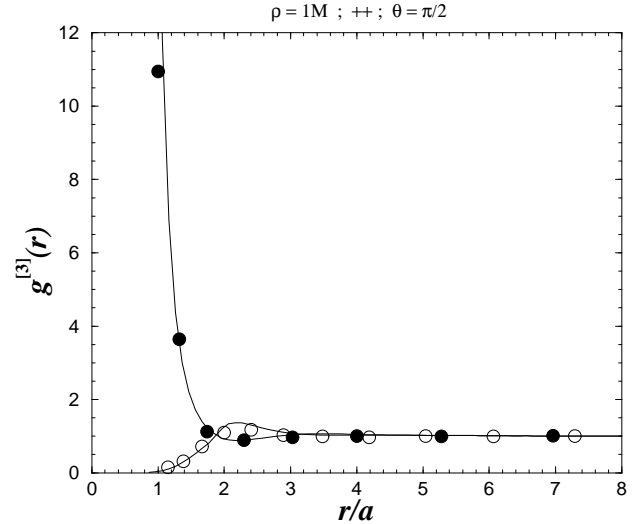


FIG. 4: Three particle distribution function $g_{+i}^{[3]}(r; \theta = 2; \theta = a)$ for a dumbbell made of two (divalent) positive particles, with $\rho = 1\text{M}$ and $z = 2$. The solid lines represent the results from TPE–HNC/M SA. The MD results are shown in filled and open circles for $g_{++}^{[3]}(r; \theta = 2; a)$ and $g_{++}^{[3]}(r; \theta = 4; a)$ respectively.

electrostatic interaction between the dumbbell and the counterion is higher at $\tau = a$. For the dumbbell-counterion distribution $g_{++}^{[3]}(r; \tau = a)$ we have quantitative agreement between TPE and MD.

The three dimensional (3D) plots of the three particle (counterion-dumbbell) distribution function $g_{++}^{[3]}(r; \tau)$ obtained by TPE-HNC/M SA are sketched in Fig. 6. At $\tau = a$ (dumbbell ions at contact), Fig. 6(a) shows a strong variation near to the surface of closest approach. As expected, the maximum is obtained at $\tau = 2a$ ($g_{++}^{[3]} = 50$), whereas the minimum is at $\tau = 0$ ($g_{++}^{[3]} = 8$). Moreover, we have oscillations in the distribution function for any τ , which confirms our previous observations at $\tau = 2a$ (see Figs. 4 and 5). We have carefully checked that this feature holds at any τ . The 3D plot of the counterion-dumbbell distribution $g_{++}^{[3]}(r; \tau)$ is not reported here. At a larger dumbbell separation, $\tau = 2a$ [see Fig. 6(b)], $g_{++}^{[3]}(r; \tau = 2a)$ is still highly peaked at $\tau = 2a$ and has its maximum value at the middle point of the dumbbell. At sufficiently large separation, we have a more isotropic counterion distribution around each dumbbell particle (not reported here).

b. Antisymmetric dumbbell We now consider antisymmetric dumbbells made of two opposite divalent ions. In this case, by symmetry arguments we have $g_{++}^{[3]}(r; \tau = 2a) = g_{+-}^{[3]}(r; \tau = 2a)$. The profiles of $g_{++}^{[3]}(r; \tau = 2a)$ and $g_{+-}^{[3]}(r; \tau = 2a)$ are plotted in Fig. 7. Since at $\tau = 2a$ the electric field component (produced by the dumbbell) perpendicular to the dumbbell axis is zero, the electrostatic correlations are only generated by the uid ions. Consequently, given that the present system is highly screened, we expect a quasi-uncorrelated neutral uid behavior. This is precisely what Fig. 7 shows for theory and simulation. Nevertheless, a slight

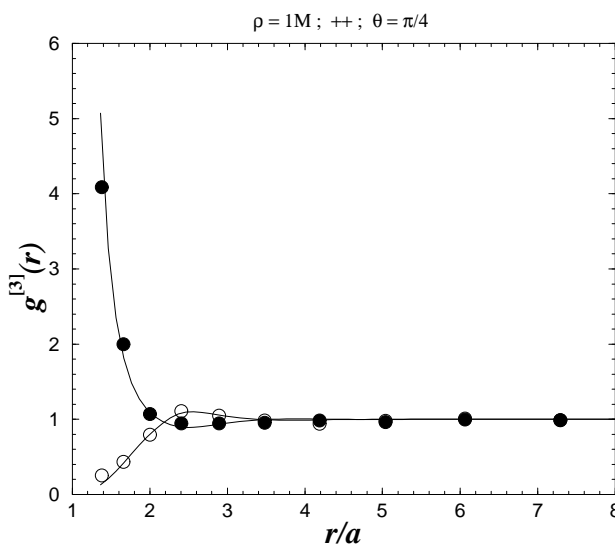


FIG. 5: Same as in Fig. 4 with $\tau = 4a$.

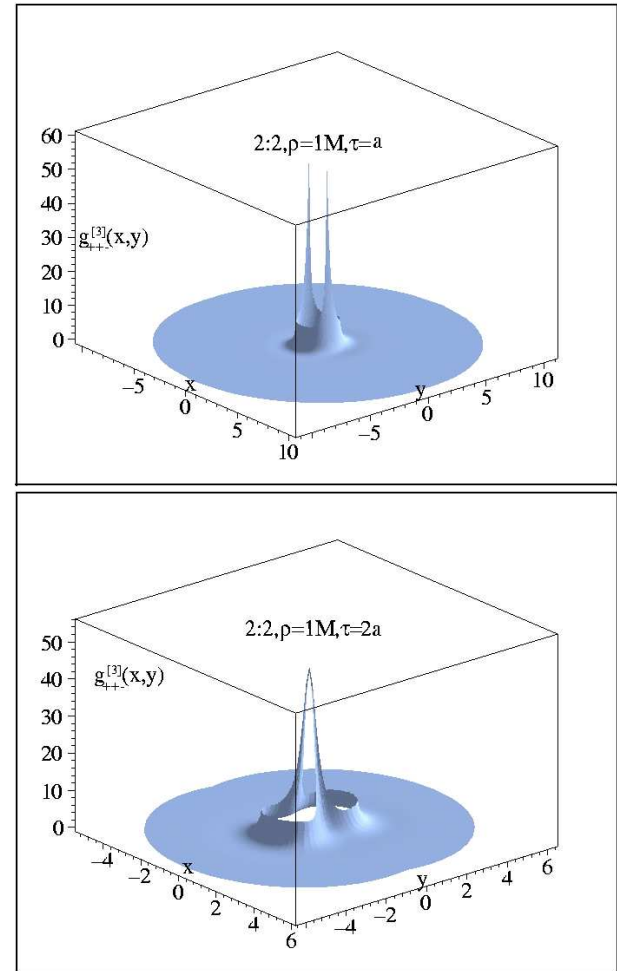


FIG. 6: 3D representation (in Cartesian coordinates) of: (a) (upper 3D plot) $g_{++}^{[3]}(r; \tau = a)$ and (b) (lower 3D plot) $g_{++}^{[3]}(r; \tau = 2a)$ obtained by TPE-HNC/M SA for the same uid parameters as in Figs. 4 and 5. The dumbbell axis is parallel to y axis.

attraction near contact is observed. This effect can be again explained with simple electrostatic arguments. The basic mechanism is the (attractive) electrostatic correlation between opposite uid charges (lying at $\tau = 2a$) located on each side of the side of the dumbbell plane.

Results for $\tau = 4a$ are shown in Fig. 8. We have again a very satisfactory agreement between theory and simulation, and this holds for the two ionic species. The 3D plot of $g_{++}^{[3]}(r; \tau = 4a) = g_{+-}^{[3]}(r; \tau = 4a)$ obtained by TPE-HNC/M SA is sketched in Fig. 9. The maximum and minimum are located at $\tau = 0$ and $\tau = 4a$ at dumbbell contact. Again, we observe oscillations at any angle, and we checked that it is the case for any τ .

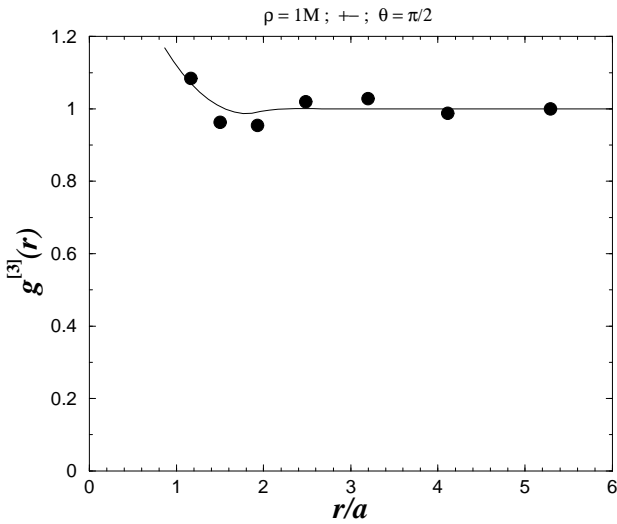


FIG. 7: Three particle distribution function $g_{+-}^{[3]}(r; \theta = \pi/2)$ for a dumbbell made of a positive and a negative divalent ions, with $\rho = 1M$ and $z = 2$. The solid lines represent the results from TPE-HNC/M SA. The MD results are shown in filled circles.

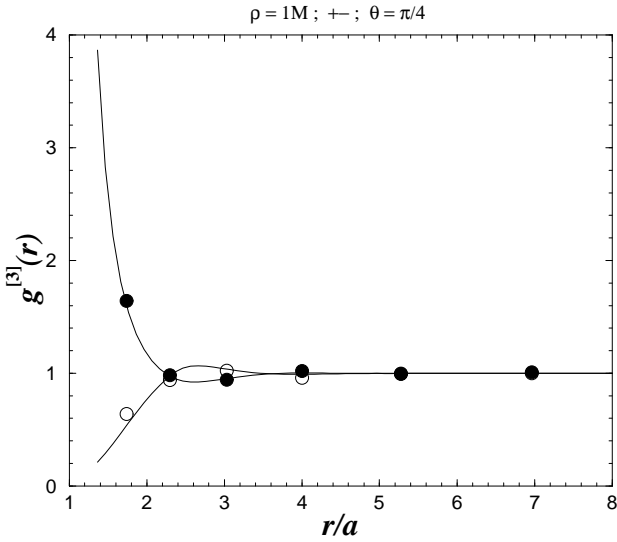


FIG. 8: Same as in Fig. 7 with $\theta = \pi/4$. The MD results are shown in filled and open circles for $g_{+-}^{[3]}(r; \theta = \pi/4; a)$ and $g_{+-}^{[3]}(r; \theta = \pi/4; a)$ respectively.

2. Effective force

The effective mean force between two like charges $F_{++}(r)$ and that between two opposite charges $F_{+-}(r)$ as a function of their mutual separation r are depicted in Fig. 10. As expected, theories (TPE-HNC/M SA and HNC/M SA) and simulation are in very good agreement for both forces $F_{++}(r)$ and $F_{+-}(r)$.

An interesting feature is the kink in $F_{++}(r)$ occur-

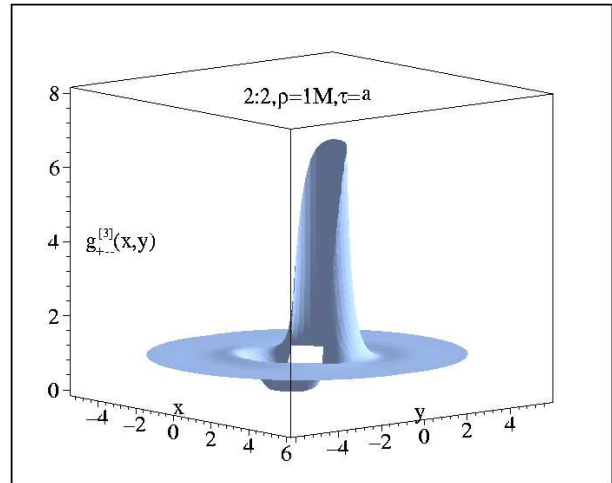


FIG. 9: 3D representation (in Cartesian coordinates) of $g_{+-}^{[3]}(x, y; a)$ obtained by TPE-HNC/M SA for the same fluid parameters as in Figs. 7 and 8. The dumbbell axis is parallel to y axis.

ring at $r = 2a$, that is somewhat less marked, however present, on the simulation plot (due to the softness of the ions and also the lower radial resolution there). This jump in the first derivative, $F_{++}^0(r)$, at $r = 2a$ is not an artifact of the theory (or the simulation) but a true physical feature. This effect is due to excluded volume correlations and in lesser degree to electrostatic correlations. It is clear that, at $r = 2a$, the conformation consisting of a counterion lying exactly between two coions

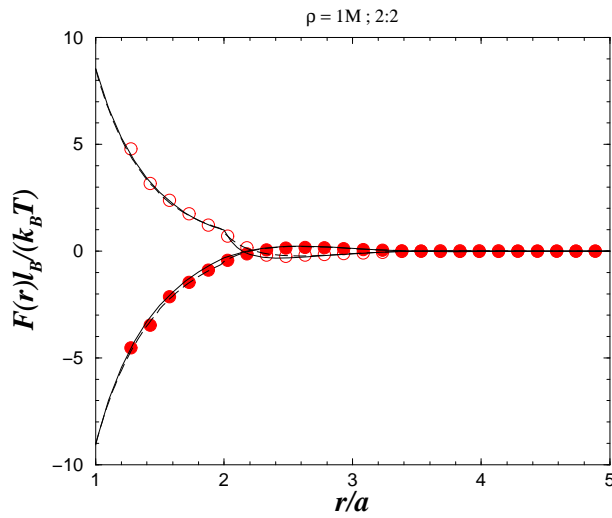


FIG. 10: Effective forces between two like charges $F_{++}(r)$ and two opposite charges $F_{+-}(r)$ as a function of their separation r , with $\rho = 1M$ and $z = 2$. The solid lines represent the results from TPE-HNC/M SA and the dashed lines are the results from HNC/M SA. The MD results are shown in filled and open circles for $F_{+-}(r)$ and $F_{++}(r)$, respectively.

(ie, $+$ $+$) is energetically very favorable. When $r > 2a$ (more precisely $r > 2a^+$), the presence of an in-between counterion leads to a relatively strong resistance, on the level of the depletion force, upon approaching the two cations. On the other hand, when $r < 2a$ (more precisely $r < 2a^+$), the absence of an in-between counterion leads to an easier approach (on the level of the depletion force) of the two cations. These mechanisms, explain (i) the discontinuity of $F_{++}^0(r)$ at $2a$ and (ii) the fact that $F_{++}^0(r < 2a) < F_{++}^0(r > 2a^+)$. This effect should also be observed in neutral hard spheres systems at sufficiently high density.

As far as the force $F_{++}(r)$ is concerned, this kind of discontinuity in the derivative is absent or nearly unde-

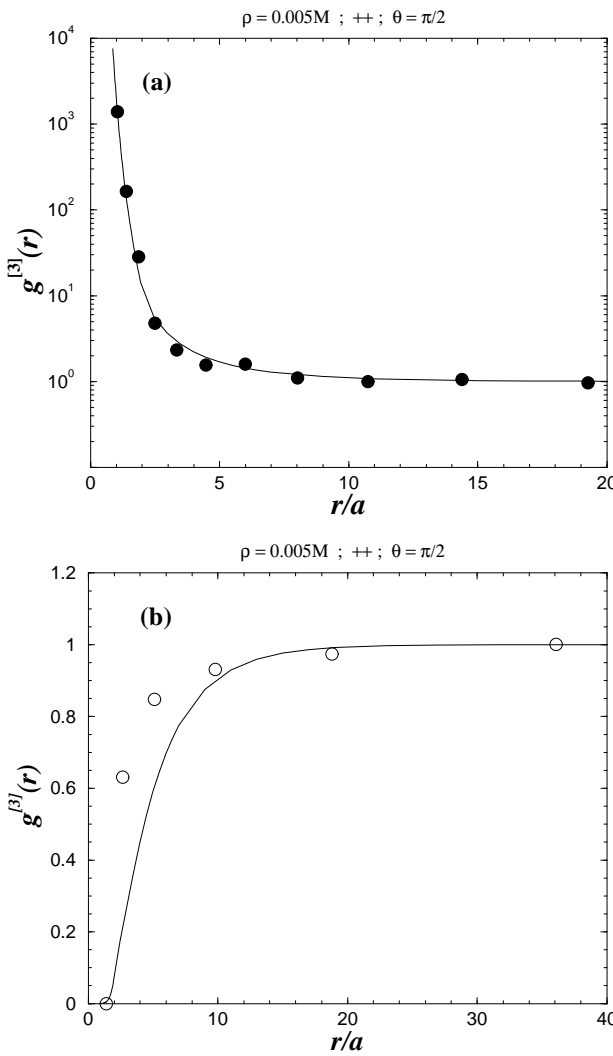


FIG. 11: Three particle distribution function with $\rho = 0.005M$ and $z = 2$: (a) $g_{++}^{[3]}(r; \theta = \pi/2; a)$ and (b) $g_{++}^{[3]}(r; \theta = \pi/2; a)$. The solid lines represent the results from TPE-HNC/MSA. The MD results are shown in filled and open circles for (a) $g_{++}^{[3]}(r; \theta = \pi/2; a)$ and (b) $g_{++}^{[3]}(r; \theta = \pi/2; a)$, respectively.

tectable. This is due to the fact that, at $r = 2a$, the probability of finding the configuration consisting of an ion between two oppositely ions (ie, $+$ $-$) is considerably smaller compared to that obtained with the configuration $+$ $+$.

B. Dilute case

In this section, we deal with the dilute case ($\rho = 0.005M$) and divalent ions ($z = 2$). Most of the usual liquid theories fail to describe its behavior under these conditions [24, 47]. Hence, the study of low concentrated solutions of multivalent ions represents a strong test case for a liquid theory.

1. Three particle correlation function

a. Symmetric dumbbell Figures 11(a) and 11(b) show a comparison between TPE and MD results for $g_{++}^{[3]}(r; \theta = \pi/2; a)$ and $g_{++}^{[3]}(r; \theta = \pi/2; a)$, respectively. One can see that the electrical double layer is wider than in the concentrated case i.e., the correlations are long ranged. For $g_{++}^{[3]}(r; \theta = \pi/2; a)$ [see Fig. 11(a)], TPE and MD results show quantitative agreement, even near contact. For the $g_{++}^{[3]}(r; \theta = \pi/2)$ [see Fig. 11(b)], a qualitative agreement between TPE and MD results is found.

At $\theta = \pi/4$ (see Fig. 12) it is found that the contact value of $g_{++}^{[3]}(r; \theta = \pi/4; a)$ (about 500) is much smaller, of two orders of magnitude, than that at $\theta = \pi/2$. This can be explained in terms of the electric field produced by the dumbbell at $\theta = \pi/2$ which is considerably stronger

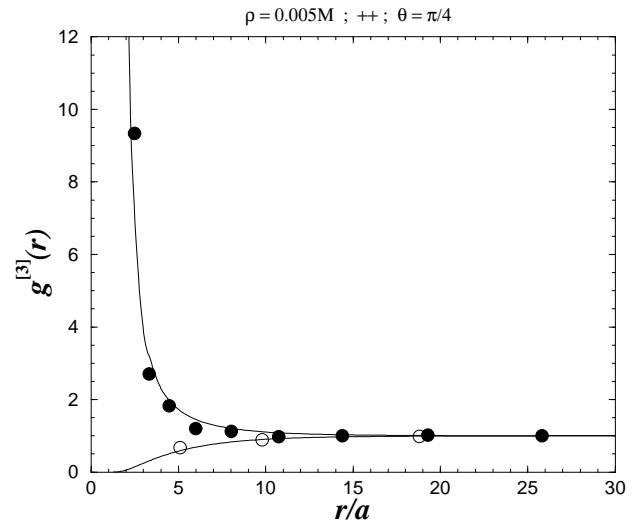


FIG. 12: Same as in Fig. 11 with $\theta = \pi/4$. The MD results are shown in filled and open circles for $g_{++}^{[3]}(r; \theta = \pi/4; a)$ and $g_{++}^{[3]}(r; \theta = \pi/4; a)$, respectively.

than at $\tau = -4$.

The 3D plot of $\ln(g_{++}^{[3]}(r; \tau; z))$ can be found in Fig. 13. For $\tau = a$ [see Fig. 13(a)], it is observed a strong variation of the distribution function close to the dumbbell (at the surface of closest approach). As expected, the maximum of $g_{++}^{[3]}(r; \tau; a)$ is at $\tau = -2$. On the other hand, at $\tau = 5a$ (see Fig. 13(b)), the angular variation of $g_{++}^{[3]}(r; \tau; 5a)$ (near contact) around one ion of the dumbbell is not as peaked as in $g_{++}^{[3]}(r; \tau; a)$. However, the dumbbell ions are still correlated, i.e., their electrical double layers are strongly overlapped although $\tau = 5a$. We had to go up to $\tau = 60a$ (not shown) to cancel the overlapping of the electrical double layers of the dumbbell ions.

b. Antisymmetric dumbbell We now consider the three particle distribution function where the dumbbell is made up of two opposite ions, and for the same uid parameters as in Figs. 11 and 12. Only the case of

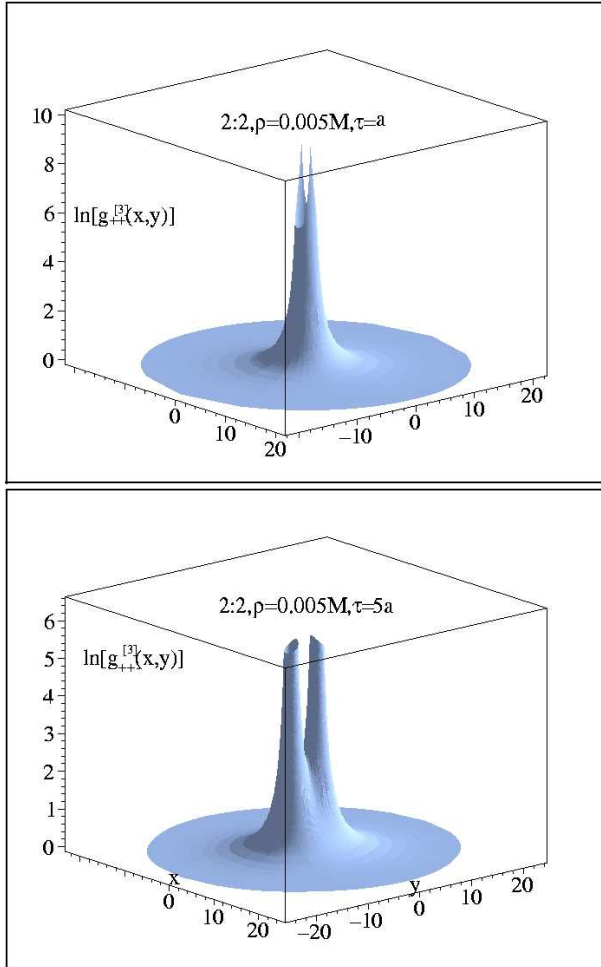


FIG. 13: 3D representation (in Cartesian coordinates) of $g_{++}^{[3]}(r; \tau; z)$ obtained by TPE-HNC/M SA for the same uid parameters as in Figs. 11 and 12. The dumbbell axis is parallel to y axis. (a) $\tau = a$ (b) $\tau = 5a$.

$\tau = -4$ is shown (see Fig. 14), given that for $\tau = -2$ the electrical field is zero and since the electrolyte concentration is very low we have $g_{++}^{[3]}(r; \tau = -2) = g_{++}^{[3]}(r; \tau = -2)$. For $\tau = -2$ the same good agreement is found between TPE and MD as that in Fig. 12.

The 3D plot of $\ln g_{++}^{[3]}(r; \tau; z = a) = \ln g_{++}^{[3]}(r; \tau; z = a)$ which is the potential mean force is sketched in Fig. 15. This function is quasi center-symmetric with respect to the dumbbell center. This feature is due to (i) the symmetry of the electrostatic correlations and (ii) the fact that the contribution of the excluded volume correlations (at such low density) is negligible compared to that in the concentrated case. As expected the function is strongly peaked at $r = 0$. For the concentrated case (not shown) the asymmetry is higher.

2. Effective force

The effective mean force between two like charges $F_{++}(r)$ and that between two opposite charges $F_{+-}(r)$ as a function of their mutual separation r can be found in Fig. 16. Concerning $F_{++}(r)$, theories (TPE-HNC/M SA and HNC/M SA) and simulation are in quantitative agreement.

As pointed out above, for $F_{++}(r)$ in the concentrated case, the derivative $F_{++}^0(r)$ is again discontinuous at $r = 2a$. The same mechanism proposed for the concentrated case (see Sec. IV A 2) applies here. This important feature is not captured by HNC/M SA, proving the qualitative improvement by using the TPE method. This better description stems from proper inclusion of long

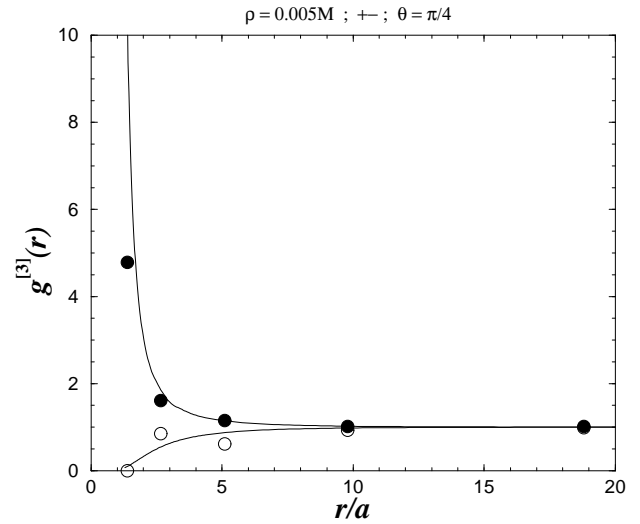


FIG. 14: Three particle distribution function $g_{++}^{[3]}(r; \tau = 4; a)$ with $\rho = 0.005M$ and $z = 2$. The solid lines represent the results from TPE-HNC/M SA. The MD results are shown in filled and open circles for $g_{++}^{[3]}(r; \tau = 4; a)$ and $g_{+-}^{[3]}(r; \tau = 4; a)$, respectively.

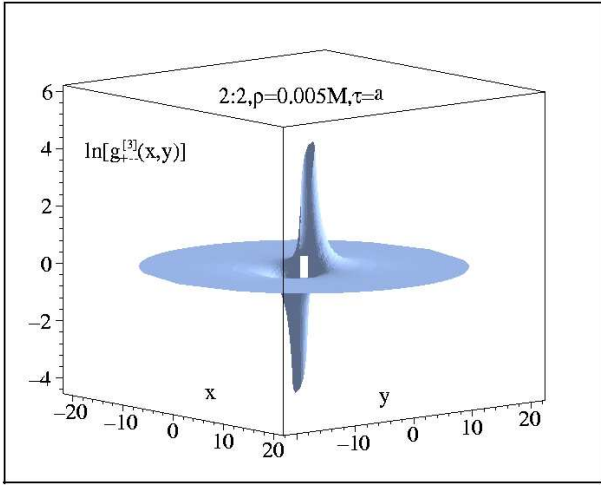


FIG. 15: 3D representation (in Cartesian coordinates) of $g_{+-}^{(3)}(r; ; a)$ obtained by TPE-HNC/M SA for the same liquid parameters as in Fig. 14. The dumbbell axis is parallel to y axis.

ranged correlations. Finally, we have an almost quantitative agreement between TPE and MD which is the main result of this work.

V. CONCLUSIONS

We have investigated the structure of 1:1 and 2:2 RPM electrolytes by means of integral equations and MD simulations. Using the three point extension to

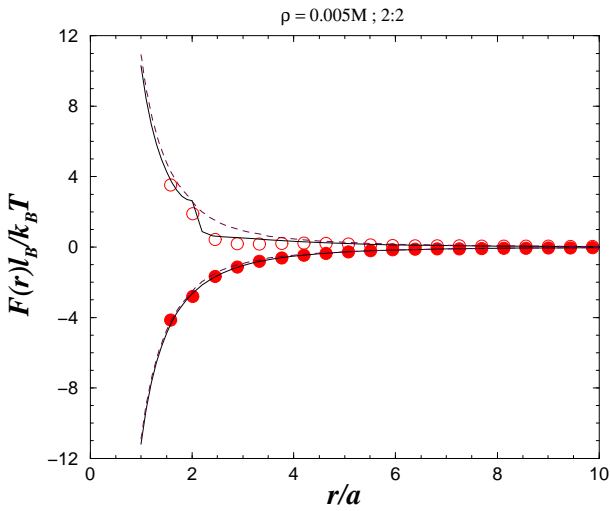


FIG. 16: Effective forces between two like charges $F_{++}(r)$ and two opposite charges $F_{+-}(r)$ as a function of their separation r , with $\rho = 0.005M$ and $z = 2$. The solid lines represent the results from TPE-HNC/M SA and the dashed lines are the results from HNC/M SA. The MD results are shown in filled and open circles for $F_{+-}(r)$ and $F_{++}(r)$, respectively.

the HNC/M SA theory, the conditional three particle distribution function, $g^{(3)}(r; ;)$, was computed and compared with that obtained by MD. Although it is not shown, for the 1:1 electrolyte the quantitative agreement between TPE and MD is excellent. For the 2:2 electrolyte, we explicitly report here results for two typical concentrations: (i) the concentrated case ($\rho = 1M$) and (ii) the dilute case ($\rho = 0.005M$).

As far as the concentrated case concerns, it was found that $g^{(3)}(r;)$ always presents oscillations. The detailed comparison between TPE and MD, carried at fixed separation $r = a$ (between the two constitutive ions of the dumbbell), shows an excellent qualitative and/or quantitative agreement. This is true for all values of ρ (not shown).

On the level of the effective mean force between two ions, both, TPE and HNC/M SA are in very good agreement with MD. This is consistent with previous comparisons between HNC/M SA and Monte Carlo results [24, 63]. Hence we can conclude that the TPE method is also suitable to describe concentrated electrolyte solutions. It is important to point out a particular behavior in the effective force between like-charged ions $F_{++}(r)$ observed at $r = 2a$, where an abrupt change in its slope appears due to excluded volume correlations. This behavior can not be directly seen in the pair distribution function (for this value of ρ).

In the dilute regime, the analysis of the three particle distribution function and the effective force shows the long range nature of the correlations. For the three particle distribution functions, we had to go up to a distance separation of $60a$, in order to uncorrelated the two constitutive dumbbell ions. Again a good agreement for $g^{(3)}(r;)$ is found between TPE and MD, proving the robustness of the TPE formalism. The study of the effective force reveals a quantitative agreement for the force between two oppositely charged ions, $F_{+-}(r)$, between TPE and MD, although HNC/M SA is also very good. For the force $F_{++}(r)$ we again remark the occurrence of an abrupt change in its slope at $r = 2a$, which is not predicted by HNC/M SA. On the other hand, TPE and MD are in quantitative agreement, showing the ability of TPE to take fairly well into account long range correlations.

The general conclusions of this work are two-fold:

In the concentrated regime, TPE is good candidate as HNC/M SA, where for this latter approach excellent agreement with molecular simulation was already reported.

In the dilute regime, TPE truly improves the description of a symmetric RPM electrolyte.

The better description (than previous theories) of strongly coupled dilute RPM electrolytes by TPE-HNC/M SA can be relevant, for example, for the study of its critical properties [64, 65]. Finally, this theory could also be successfully applied to the study of neutral hard spheres liquids.

Acknowledgments

FJA and MLC thank CONACYT (L007E and C086A) and NEGROMEX for their financial support. RM gratefully acknowledges the support of Laboratoires Européens Associés (LEA).

APPENDIX A : NUMERICAL METHOD

1. Finite Element Method

To solve the TPE-HNC/M SA equation, Eq. (22), it is necessary to use a numerical method, since an analytical solution is not available. The finite element method (FEM) has been used in the past to solve HNC/M SA equation in several geometries [32, 37, 66] and it has been proved to be efficient. The general form of TPE-HNC/M SA integral equation can be written as

$$g_i(x, y) = \exp M_i(x, y) + \sum_{m=1}^M h_m(x, y) F_m(x, y) d^0 d^0 g_i \quad (A1)$$

where $h_m(x, y)$ and $M_i(x, y)$ are functions defined on a bidimensional domain $(x, y) \in [1;1] \times [1;1]$. Since $h_m(x, y) \neq 0$ only in a region close to the dumbbell, we solve Eq. (A1) just in a finite domain. In the FEM [67], the domain is divided into N elements. Every element in a domain A_K is divided into L_0 sub-elements. In prolate coordinates, the dumbbell geometry of Fig. 17 is mapped into the geometry shown in Fig. 18, where one of the N triangular elements is shown.

In order to solve Eq. (A1), the function $h_m(x, y)$ is expanded as a linear combination of a L_0 base elements $h_i^K(x, y); i = 1, \dots, L_0$, where $1 \leq K \leq N$. These base functions are defined in such a way that $h_i^K(x, y) = 0$ if $(x, y) \notin A_K$. Furthermore the base functions are chosen so that for a set of L_0 points (ξ_j, η_j) (which are called nodes, see Fig. 18), they satisfy

$$h_i^K(x, y) = \delta_{ij} \quad \text{with } i, j = 1, \dots, L_0 \quad (A2)$$

with δ_{ij} being the Kronecker delta function. Hence,

$$h_m(x, y) = \sum_{K=1}^N \sum_{l=1}^{L_0} \delta_{ml} h_l^K(x, y) \quad (A3)$$

where $\delta_{ml}; l = 1, \dots, L_0$ are the L_0 coefficients of the h_m in the K -th finite element. Thereby, the coefficient δ_{ml} is the value of the function at the i -th node, i.e.,

$$\delta_{ml} = h_m(\xi_l, \eta_l) \quad (A4)$$

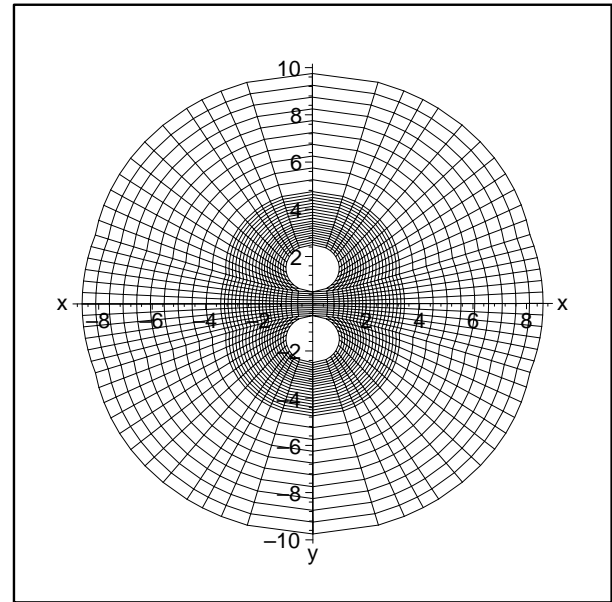


FIG. 17: An example of the grid (in Cartesian coordinates) used to solve Eq.(A1).

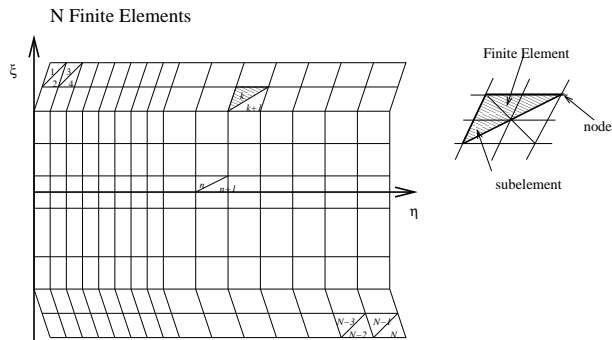


FIG. 18: The same grid as in Fig. 17 but mapped into the (ξ, η) plane. A triangular element and its 6 nodes are represented.

It is useful to renumber δ_{ml} and δ_{ml} , so that Eq. (A3) can be rewritten as follows

$$h_m(x, y) = \sum_{l=1}^{L_0} \delta_{ml} h_l(x, y) \quad (A5)$$

where

$$\delta_{ml} = h_m(\xi_l, \eta_l) = g_m(\xi_l, \eta_l) \quad (A6)$$

with $M_0 = N \times L_0$, and the superscript K has been omitted. By substituting Eq. (A5) into Eq. (A1), we get

$$g_i(x, y) = \exp M_i(x, y) + \sum_{l=1}^{L_0} \sum_{m=1}^M \delta_{ml} C_1(x, y) \quad (A7)$$

where

$$C_1(z; z) = \int_{A_K} (z; z) F(z; z) d^0 d^0: \quad (A 8)$$

Evaluating Eq. (A 7) at the k -th node $(z_k; z_k)$ and using Eq. (A 6), we get

$$!_{ik} = \exp \left(M_{ik} + \sum_{l=1}^m \sum_{m=1}^m C_{lk} \right) \quad (A 9)$$

with $C_{lk} = C_1(z_k; z_k)$ and $M_{ik} = M_i(z_k; z_k)$: Thus, we have a system of $2M_0$ non-linear algebraic equations which can be solved by any of the standard methods, for example the Newton's method, which is our method of choice.

2. Choice of the base functions $\psi_i(z; z)$

To construct the base functions, it is necessary to use a coordinate system defined in the element's domain. In our method, we have used the area coordinates (L_i) defined as follows

$$L_i = \frac{a_i + b_i + c_i}{2} \quad \text{with } i = 1, 2, 3; \quad (A 10)$$

where 2 is the area of the triangular element and

$$a_i = j_k k_j;$$

$$\begin{aligned} b_i &= j_k k_j; \\ c_i &= k_j j_k; \end{aligned} \quad (A 11)$$

with cyclic rotation of indexes, where $j, k = 1, 2, 3$ but $i \notin j \notin k$. The set of points $f(z_i; z_i); i = 1, 2, 3$ are the coordinates of the triangle corners. The relation between the coordinates $(z; z)$ and the triangular coordinates $f L_i; i = 1, 2, 3$ is given by

$$\begin{aligned} &= L_1 z_1 + L_2 z_2 + L_3 z_3; \\ &= L_1 z_1 + L_2 z_2 + L_3 z_3; \\ &= L_1 + L_2 + L_3; \end{aligned} \quad (A 12)$$

The number of nodes is equal to the number of base elements. A quadratic base was used to solve Eq. (A 1) and therefore $L_0 = 6$. For the corner nodes we have

$$1 = (2L_1 - 1)L_1; \text{etc}; \quad (A 13)$$

and for the middle-side nodes

$$4 = 4L_1 L_2; \text{etc}; \quad (A 14)$$

In this coordinate system, Eq. (A 8) becomes

$$\begin{aligned} C_1(z; z) &= \int_{0,0}^{z_1, z_1} F(L_1; L_2; z; z) dL_1 dL_2; \quad (A 15) \end{aligned}$$

[1] D. A. M. Quarrie, *Statistical Mechanics* (Harper and Row, New York, 1976).

[2] J. P. Hansen and I. R. M. McDonald, *Theory of simple liquids*, 2nd ed. (Academic Press, London, 1986).

[3] D. L. Goodstein, *States of matter* (Dover Publications Inc., New York, 1985).

[4] L. Verlet, *Phys. Rev.* 165, 201 (1968).

[5] G. M. Kepler and S. Fraden, *Phys. Rev. Lett.* 73, 356 (1994).

[6] J. C. Crocker and D. G. Grier, *Phys. Rev. Lett.* 77, 1897 (1996).

[7] M. Born and M. S. Greene, *A General Kinetic Theory of Liquids* (Cambridge University Press, Cambridge, 1949).

[8] J. Yvon, *La Theorie Statistique des Fluides et l'Equation d'Etat*, Actualites Scientifiques et Industrielles (Hermann, Paris, 1935), Vol. 203.

[9] J. G. Kirkwood, *J. Chem. Phys.* 3, 300 (1935).

[10] J. K. Percus, in *The Equilibrium Theory of Classical Fluids*, edited by H. L. Frisch and J. L. Lebowitz (W. A. Benjamin, New York, 1964), Chap. II, p. 33.

[11] G. Stell, in *The Equilibrium Theory of Classical Fluids*, edited by H. L. Frisch and J. L. Lebowitz (W. A. Benjamin, New York, 1964), Chap. II, p. 171.

[12] L. S. Ornstein and F. Zernike, *Proc. Akad. Sci. (Amsterdam)* 17, 793 (1914).

[13] F. Zernike, *Proc. Akad. Sci. (Amsterdam)* 18, 1520 (1916).

[14] M. Metropolis et al., *J. Chem. Phys.* 21, 1087 (1953).

[15] B. J. Alder and T. E. Wainwright, *J. Chem. Phys.* 31, 459 (1959).

[16] D. Henderson, *Annu. Rev. Phys. Chem.* 15, 31 (1964).

[17] T. L. Croxton and D. A. M. Quarrie, *J. Phys. Chem.* 83, 1840 (1979).

[18] R. Evans, in *Fundamentals of Inhomogeneous Fluids*, edited by D. Henderson (Marcel Dekker Inc., New York, 1992), Chap. 3, p. 85.

[19] P. Hohenberg and W. Kohn, *Phys. Rev.* 136, B864 (1964).

[20] W. Kohn and L. J. Sham, *Phys. Rev.* 140, A1133 (1965).

[21] J. K. Percus and G. J. Yevick, *Phys. Rev.* 110, 1 (1958).

[22] G. S. Rushbrooke and H. I. Scoins, *Proc. Roy. Soc.* 216A, 203 (1953).

[23] J. L. Lebowitz and J. Percus, *Phys. Rev.* 144, 251 (1966).

[24] D. Henderson, M. Lozada-Cassou, and L. Blum, *J. Chem.*

Phys. 79, 3055 (1983).

[25] J. K. Percus, Phys. Rev. Lett. 8, 462 (1962).

[26] H. L. Friedman, *A Course in Statistical Mechanics* (Prentice Hall, Englewood Cliffs, NJ, 1985).

[27] M. Lozada-Cassou, in *Fundamentals of inhomogeneous fluids*, edited by D. Henderson (Marcel Dekker, New York, 1993), Chap. 8.

[28] M. Lozada-Cassou, J. Chem. Phys. 75, 1412 (1981).

[29] In this way, integral equations theories for inhomogeneous fluids are derived in an straightforward manner.

[30] M. Lozada-Cassou, J. Chem. Phys. 80, 3344 (1984).

[31] M. Lozada-Cassou and E. D. az-Herrera, J. Chem. Phys. 92, 1194 (1990).

[32] M. Lozada-Cassou and E. D. az-Herrera, J. Chem. Phys. 93, 1386 (1990).

[33] J. A. lejandre, M. Lozada-Cassou, E. G. Gonzalez-Tovar, and G. A. Chapela, Chem. Phys. Lett. 172, 111 (1990).

[34] M. Lozada-Cassou, W. Olivares, and B. Sulbaran, Phys. Rev. E 53, 522 (1996).

[35] J. P. Valleur, R. Ivkov, and J. M. Torrie, J. Chem. Phys. 95, 520 (1991).

[36] S. L. Cramie and D. Chan, J. Colloid Interface Sci. 155, 297 (1992).

[37] J. E. Sanchez and M. Lozada-Cassou, Chem. Phys. Lett. 190, 202 (1992).

[38] K. S. Schmitz, *Macroions in Solution and Colloidal Suspensions* (VCH Publishers, New York, 1993).

[39] S. L. Cramie, D. Chan, and J. Stankovich, J. Colloid Interface Sci. 165, 116 (1993).

[40] J. C. Rasaiah and H. L. Friedman, J. Chem. Phys. 50, 3965 (1969).

[41] J. C. Rasaiah, Chem. Phys. Lett. 7, 260 (1970).

[42] J. C. Rasaiah, J. Chem. Phys. 56, 3071 (1972).

[43] E. W. Saini and J. L. Lebowitz, J. Chem. Phys. 56, 3086 (1972).

[44] E. W. Saini and J. L. Lebowitz, J. Chem. Phys. 56, 3093 (1972).

[45] D. N. Card and J. P. Valleur, J. Chem. Phys. 52, 6232 (1970).

[46] J. C. Rasaiah, Chem. Phys. Lett. 7, 260 (1970).

[47] S. A. Rogde and B. Hafskjold, Mol. Phys. 48, 1241 (1983).

[48] R. Bacquet and P. J. Rossky, J. Chem. Phys. 79, 1419 (1983).

[49] T. Ichijo and A. D. J. Haymet, J. Chem. Phys. 89, 4315 (1988).

[50] T. Ichijo and A. D. J. Haymet, J. Chem. Phys. 93, 8954 (1990).

[51] V. Vlachy, T. Ichijo, and A. D. J. Haymet, J. Am. Chem. Soc. 113, 1077 (1991).

[52] D. M. Duh and A. D. J. Haymet, J. Chem. Phys. 97, 7716 (1992).

[53] R. Kjellander and S. M. Arcelia, Mol. Phys. 83, 789 (1994).

[54] M. P. Lischke and D. Henderson, J. Phys. Chem. 92, 7177 (1988).

[55] M. P. Lischke and D. Henderson, Electrochim. Acta 34, 1863 (1989).

[56] P. Attard, J. Chem. Phys. 91, 3072 (1989).

[57] P. Attard, J. Chem. Phys. 91, 3083 (1989).

[58] G. Arfken, *Mathematical Methods for Physicists* (Academic Press Inc., San Diego, CA, 1985).

[59] R. Messina, C. Holm, and K. Kremser, Phys. Rev. Lett. 85, 872 (2000).

[60] R. Messina, C. Holm, and K. Kremser, Europhys. Lett. 51, 461 (2000).

[61] R. Messina, C. Holm, and K. Kremser, Phys. Rev. E 64, 021405 (2001).

[62] M. Deserno and C. Holm, J. Chem. Phys. 109, 7678 (1998).

[63] L. Degreve, M. Lozada-Cassou, E. Sanchez, and E. Gonzalez-Tovar, J. Chem. Phys. 98, 8905 (1993).

[64] M. E. Fisher, J. Stat. Phys. 75, 1 (1994).

[65] Y. Levin and M. E. Fisher, Physica A 225, 164 (1996).

[66] L. Mier y Teirán, E. D. az-Herrera, M. Lozada-Cassou, and R. Saavedra-Barrera, J. Comp. Phys. 84, 326 (1989).

[67] O. C. Zienkiewicz and R. L. Taylor, *The Finite Element Method*, 4th ed. (McGraw Hill Book Company, London, 1989), Vol. 1.